Title

Polymeric perfluorocarbon nanoemulsions are ultrasound-activated wireless drug infusion catheters

Authors

Zhong, Q
Yoon, BC
Aryal, M
et al.

Publication Date

2019-06-01

DOI

10.1016/j.biomaterials.2019.03.021

Peer reviewed

HHS Public Access

Author manuscript

Biomaterials. Author manuscript; available in PMC 2020 June 01.

Published in final edited form as:

Biomaterials. 2019 June ; 206: 73–86. doi:10.1016/j.biomaterials.2019.03.021.

Polymeric perfluorocarbon nanoemulsions are ultrasound-activated wireless drug infusion catheters

Q Zhong[†,1,2], **BC Yoon**[†,1,3], **M Aryal**[1], **JB Wang**[1], **T Ilovitsh**[1,4], **MA Baikoghli**[5], **N Hosseini-Nassab**[1], **A Karthik**[1], **RH Cheng**[5], **KW Ferrara**[1,4], and **RD Airan**[1,*]

[1]Department of Radiology, Stanford University, Stanford, CA 94305, U.S.A.

[2]David H. Koch Institute for Integrative Cancer Research, Massachusetts Institute of Technology, Cambridge, MA 02142

[*]To whom correspondence should be addressed: Raag Airan MD PhD, Departments of Radiology (Neuroradiology) and, by courtesy, Materials Science & Engineering, Stanford University, 300 Pasteur Drive, Grant Rm. S043, Stanford, CA 94305, Office: 650-724-1190, Fax: 650-736-6767, rairan@stanford.edu.

Author Contributions

QZ and RDA designed the experiments. QZ performed the chemistry of nanoparticle production and physicochemical characterization, carried out the pharmacokinetics study and *in vivo* biodistribution of the nanoparticles, and performed the *in vitro/in vivo* ultrasonic drug uncaging experiments, with guidance from MA and assistance from JBW and AK. Cryo-TEM imaging was performed by MAB, RHC, and NHN. QZ and BCY performed the ultrasound imaging and ultrasonic nicardipine uncaging experiments and their analysis. TI and KFW designed and performed the ultra-high-speed optical imaging and passive cavitation detection of the nanoemulsions. QZ, BCY, and RDA prepared the figures and wrote the manuscript, with input and edits from all the authors.

[†]These authors contributed equally to this work.

Data Availability Statement

The raw data required to reproduce these findings will be available to download from http://airan-lab.stanford.edu/publications/. The processed data required to reproduce these findings will be available to download from http://airan-lab.stanford.edu/publications/.

Supporting Information

The Supporting Information is available free of charge on http://pubs.acs.com

- Supplementary methods for dynamic light scattering, drug loading quantification, endotoxin assay, and LB agar plate tests.
- Figure S1: Typical dynamic light scattering spectrum of the propofol-loaded PFP polymeric nanoemulsion;
- Figure S2: Physicochemical properties of polymeric nanoemulsions with varied volume ratios of PFP to nanoparticle;
- Figure S3: Effect of particle size on *in vitro* uncaging efficacy of propofol-loaded nanoemulsions;
- Figured S4–S5: Physicochemical property changes of propofol-loaded nanoemulsions (1) after frozen storage; (2) across freeze-thaw cycles; (3) after thawing;
- Figure S6: Modeling of blood-pool kinetics of the nanoemulsions after bolus administration;
- Figure S7: *In vitro* ultrasonic drug uncaging with 270 kHz sonication;
- Figure S8: Blood flow velocity changes after ultrasonic nicardipine uncaging in the aorta;
- Tables S1–S3: Tables summarizing plasma and whole blood half-lives of nanoemulsions and ultrasonically uncaged model drugs.
- Supplementary Videos S1 and S2: Videos demonstrating the distension of the abdominal aorta upon ultrasonic nicardipine uncaging.

Competing Interests

Patent applications have been filed on inventions described in this manuscript (17–163 – Provisional application with Stanford University; QZ and RDA) and on related technology (PCT/US2017/033226 with Johns Hopkins University; RDA).

[3]Department of Radiology, Massachusetts General Hospital, Boston, MA 02114

[4]Department of Biomedical Engineering, University of California, Davis, CA 95616, U.S.A.

[5]Department of Molecular and Cellular Biology, University of California, Davis, CA 95616, U.S.A

Abstract

Catheter-based intra-arterial drug therapies have proven effective for a range of oncologic, neurologic, and cardiovascular applications. However, these procedures are limited by their invasiveness and relatively broad drug spatial distribution. The ideal technique for local pharmacotherapy would be noninvasive and would flexibly deliver a given drug to any region of the body with high spatial and temporal precision. Combining polymeric perfluorocarbon nanoemulsions with existent clinical focused ultrasound systems could in principle meet these needs, but it has not been clear whether these nanoparticles could provide the necessary drug loading, stability, and generalizability across a range of drugs, beyond a few niche applications. Here, we develop polymeric perfluorocarbon nanoemulsions into a generalized platform for ultrasound-targeted delivery of hydrophobic drugs with high potential for clinical translation. We demonstrate that a wide variety of drugs may be effectively uncaged with ultrasound using these nanoparticles, with drug loading increasing with hydrophobicity. We also set the stage for clinical translation by delineating production protocols that are scalable and yield sterile, stable, and optimized ultrasound-activated drug-loaded nanoemulsions. Finally, we exhibit a new potential application of these nanoemulsions for local control of vascular tone. This work establishes the power of polymeric perfluorocarbon nanoemulsions as a clinically-translatable platform for efficacious, noninvasive, and localized ultrasonic drug uncaging for myriad targets in the brain and body.

Keywords

Focused ultrasound; Clinically translatable; Targeted drug delivery; Noninvasive ultrasonic drug uncaging; Drug delivery platform; Spatiotemporally controlled release

1. Introduction

Many clinical therapies utilize intra-arterial catheter infusion of a drug [1–3] to maximize the therapeutic effect at the target, while minimizing side effects due to drug action in the non-targeted organ and body. However, these catheter-based therapies cannot necessarily achieve the desired spatial precision for a given case, due to limitations in reliably directing a catheter into a target small artery. Additionally, endovascular catheter-based therapies are invasive interventions that carry additional risks of vascular injury, as well as of radiation as they are usually guided by real-time fluoroscopy [4]. Ideally, local pharmacotherapy would be achieved noninvasively and with image-guidance that does not involve ionizing radiation, such as with optical [5–7], ultrasound [8,9], or MRI [10,11] based methods. An ultrasound-gated mechanism of action would be particularly useful, given the availability of clinical MRI- or optically-guided focused ultrasound systems that may sonicate nearly any region of the body with millimetric spatial resolution, especially for lower intensity ultrasound applications [12].

Importantly, several ultrasound-sensitive drug delivery systems have been described. These technologies may use nano- or micro-scale drug carriers that release a drug after ultrasound raises the *in situ* temperature [13,14], activates a 'sonosensitizer' [15], or applies a sufficient peak intensity or pressure [9,16,17]. While high-intensity continuous wave ultrasound (for temperature-gated systems) may be difficult to achieve stably or specifically in certain regions of the body (e.g. skull-adjacent parts of the brain) [18], raising the peak pressure or intensity necessitates only short bursts of ultrasound that are more straightforward to achieve *in situ*.

Perfluorocarbon nanoemulsions offer several features that are optimal for this application of noninvasive localized ultrasound-mediated drug delivery: an intensity/pressure-gated drug release that should be generally applicable across a range of drugs. Indeed, such nanoemulsions have been used in preliminary proof-of-concept studies for delivering therapeutics to tumors [19,20], for diagnosis of tumors [21], and for delivery of the anesthetic propofol to the brain [22,23], with drug release induced by short pulses of sonication of a sufficient intensity. However, important questions have persisted as to whether these nanoemulsions could achieve the drug loading, generalizability of drug encapsulation, and stability [19] necessary for applications beyond those few niche, proof-of-concept studies. Additionally, it has been unclear whether these particles could be produced in a manner that would enable eventual clinical translation. Finally, given the relatively large size of these nanoparticles that limits their penetration into organs, the ultrasound-induced drug release would occur in the blood vessels, and doubts have existed as to whether intravascular drug release from these particles would truly result in a localized drug action. Here, we develop this system to address each of these open questions and explicitly demonstrate the versatility of this platform for ultrasonic uncaging of a variety of drugs, with production methods, *in vivo* biodistribution, and pharmacokinetics that enable clinical translation. Additionally, we observe no cavitation during drug uncaging, underlining the safety of this technique. Further, we demonstrate that this technology can achieve drug release that is localized in space and time to the ultrasound field, while exhibiting this localized pharmacologic modulation in the highest flow vessel of the body, the aorta. Together, these results indicate that ultrasound-induced noninvasive intravascular nanoparticle uncaging is indeed a viable and readily translatable system for local pharmacotherapy for a range of organ systems.

2. Materials and methods

2.1 Materials

Di-block copolymers are made up of a hydrophilic block of polyethylene glycol (PEG; mol. wt. 2 kDa) and a hydrophobic block of one of: poly(lactic-co-glycolic acid) (PLGA), poly(L-lactic acid) (PLLA), or poly(ε-caprolactone) (PCL). Two molecular weights of hydrophobic block chains were used: 2 kDa and 5 kDa. The nomenclature used for the di-block copolymers is, for instance, polyethylene glycol 2 kDa - poly(lactic-co-glycolic acid) 5 kDa = PEG (2 kDa)-PLGA (5 kDa). All di-block copolymers were purchased from Akina (West Lafayette, IN, USA). Propofol, nicardipine hydrochloride, verapamil hydrochloride, sodium sulfate, and sodium hydroxide were purchased from Alfa Aesar (Haverhill, MA,

USA). Doxorubicin hydrochloride was purchased from LC laboratories (Woburn, MA, USA). Cisplatin, dexmedetomidine, Luria Broth (LB) powder, and LB agar powder were purchased from Sigma-Aldrich (St Louis, MO, USA). Ketamine hydrochloride injectable solution is a controlled substance and was purchased via Stanford University Environmental Health & Safety. Tetrahydrofuran (THF), methanol, ethyl acetate, chloroform, and hexane were obtained from Sigma-Aldrich (St Louis, MO, USA). n-Perfluoropentane (PFP) was purchased from FluoroMed (Round Rock, TX, USA). A hydrophobic IRDye® 800RS infrared dye was purchased from LI-COR Biotechnology (Lincoln, NE, USA).

2.2 Production of drug-loaded polymeric perfluoropentane nanoemulsions

The production of polymeric perfluoropentane (PFP) nanoemulsions was similar for all the tested drugs and amphiphilic di-block copolymers. Briefly, 150 mg of di-block copolymer and 15 mg of drug with hydrochloride removed (if necessary; see Method S1 in Supporting Information) were weighed into a 20 ml glass beaker and 10 ml THF was added to dissolve the polymer and drug. Then, 10 ml phosphate buffer saline (PBS) was added dropwise to the organic solution over 5 min. The THF was fully evaporated by placing the mixture overnight in atmosphere and then in vacuum for 1 h. Then, 300 μl cold PFP (volume fraction = 3% relative to micelle solution) was added to the micelle solution, followed by 5 min sonication in a 40 kHz Bransonic M1800H bath sonicator (Thermo Scientific; Waltham, MA, USA) which was pre-filled with ice water. The resulting nanoparticles were washed three times and collected by centrifugation (2000 rcf) for a total of 10 min at 4 °C. Finally, the nanoemulsion suspension was extruded using an Avestin Liposofast LF-50 extruder (Ottawa, ON, Canada) with compressed nitrogen (40–100 psi) and loaded with a Nuclepore Track-Etch polycarbonate membrane (0.6 μm pores; GE Healthcare, Chicago, IL, USA). The extruded nanoemulsion suspension was either used fresh or mixed with glycerin (2.25%, w/v) and frozen immediately and stored at −80 °C.

2.3 Physicochemical characterization of drug-loaded polymeric perfluoropentane nanoemulsions

The Z-average diameter, polydispersity index (PDI) and zeta potential of the drug-loaded phase-change nanoemulsions were measured with a Malvern Zetasizer Nano ZS90 (Malvern, United Kingdom). The drug loading in the nanoemulsion was quantified with either UV absorption or fluorescence (details in Method S2–3 of Supporting Information). Cryo-electron microscopy (Cryo-EM) was performed on a JEOL JEM 2100F cryo-TEM (Peabody, MA, USA; see Supporting Information S4 for details). Endotoxin concentration of the propofol-loaded nanoemulsion was assayed with ToxinSensor™ LAL endotoxin kit (GenScript. NJ, USA) following the provided protocol (Protocol: L00350; Supporting Information S5). According to the US Food and Drug Administration, ≤5 EU/mg drug is considered an acceptable endotoxin concentration given an intended drug dose of 1 mg/kg [24]. The sterility of the propofol-loaded nanoemulsion was evaluated by plating on LB agar plates and assessing colony growth at 72 h of incubation at 37 °C (see Supporting Information S6 for details).

2.4 Nanoemulsion stability at varied temperatures.

Propofol-loaded nanoemulsions were used to assess the particle stability at different temperatures. Z-average size, polydispersity index, and free propofol content in the nanoemulsion were evaluated after frozen storage at −80 °C and at 0 °C (i.e. stored on ice), after thaw. The nanoemulsion was assessed after 7, 15, and 30 days in storage at −80 °C. After thaw from −80 °C, the above-mentioned physicochemical parameters were assessed at 45 min and 3 hrs after thaw. The effect of nanoemulsion concentration (as indexed by drug concentration) on particle stability during storage was also assessed. The initial concentration of propofol in the nanoemulsion was selected as either 0.5, 1, or 3 mg/ml by adjusting the resuspension PBS volume during nanoemulsion production. Finally, the effects of repeated freeze-thaw cycles on the integrity of the nanoemulsions was assessed. The nanoemulsion was thawed as described above and then frozen shortly after sampling. Up to five freeze-thaw cycles were performed consecutively.

2.5 In vitro assay of ultrasonic drug uncaging

Polymer and drug hydrophobicity are believed to play a critical role in the physicochemical properties and the drug uncaging efficiency of these nanoparticles. We therefore studied the effect of polymer composition and drug partition coefficient (LogP, a measure of hydrophobicity of a molecule; the drug is hydrophobic if LogP > 0 and hydrophilic if LogP < 0) on *in vitro* drug uncaging from the nanoemulsions. Propofol was used as a model drug to study the effect of varying the hydrophobic polymer blocks. A 50 μl nanoemulsion suspension (1 mg/ml encapsulated drug equivalent) was added to a Fisherbrand™ 0.2 ml PCR tube (Fisher Scientific. NJ, USA). A 150 μl organic solvent of density less than water (notably, the solvents used here do not dissolve or disrupt the polymer) was added on top of the nanoemulsion suspension. The choice of solvent varied depending on the drug being tested: hexane was used to extract propofol and ketamine; ethyl acetate was used for nicardipine, verapamil, dexmedetomidine, and doxorubicin. The PCR tube was placed in a custom holder and coupled using degassed water to a focused ultrasound (FUS) transducer (Image Guided Therapy, Pessac, France) at room temperature, so that the FUS focus was contained within the nanoemulsion suspension layer. The nanoemulsions were sonicated with FUS for 60 s total, with varying peak negative pressure, using cycles of 50 ms ultrasound on and 950 ms off, i.e. pulse repetition frequency of 1 Hz. The center frequency of the transducer was 270 kHz, 650 kHz, or 1.5 MHz. Following FUS, 100 μl of the organic solution was collected without disturbing the aqueous layer. The amount of the uncaged drug was quantified by measuring its UV absorbance or fluorescence and comparing to a standard curve of the drug prepared to varying concentrations in the same organic solvent. PEG (2 kDa)-PLGA (5 kDa) was used to create all nanoemulsions for the analysis of how the drug LogP affects nanoemulsion characteristics. The experimental setup and procedure were otherwise similar.

2.6 Pharmacokinetics and biodistribution of drug-loaded polymeric PFP nanoemulsions

All animal experiments were carried out in accordance with the Stanford IACUC. Long-Evans rats with initial body weight 180–200 g (Charles River Laboratories, Wilmington, MA, USA) were used in all *in vivo* studies. Drug-loaded PFP/PEG (2 kDa)-PLGA (5 kDa)

nanoemulsions were doped with a hydrophobic near infrared fluorescent dye, IR800, during nanoemulsion production. Propofol, nicardipine, and doxorubicin-loaded nanoemulsions were used to test *in vivo* blood-pool nanoparticle kinetics and systemic biodistribution.

To produce dye-doped nanoemulsions, 1 mg IR800 dye was added to the drug and polymer THF solution (1:15 dye:drug ratio), and the rest of the nanoemulsion production protocol was unchanged. For the experiments, a nanoemulsion bolus (equivalent to 1 mg/kg of drug) was administered intravenously via a 24 g × ¾" catheter to rat tail vein in a total volume of ~0.4–0.5 ml (N=3). Blood samples were collected via the left or right submandibular vein at 2 min 10 min, 20 min, 40 min, 2 h and 4 h, alternating sides for each sampling. The blood was split into two volumes. Whole blood sample fluorescence was assessed using a Lago (Spectral Instruments Imaging; Tucson, AZ, USA) imaging system (excitation/emission = 770/810 nm) and quantification was completed using regions of interest (ROIs) of the same size across samples, drawn to be within the capillary tube. The second volume of each sample was centrifugated in a microcentrifuge for a total of 10 min at 10,000 g at 4 °C. The plasma fraction from these samples was then collected and their fluorescence was quantified similar to that of the whole-blood samples. The nanoemulsion concentrations in the whole blood and plasma were fitted with a two-compartment kinetic model. The clearance kinetics of dye-doped propofol-loaded nanoemulsions administered as a bolus (equivalent to 1 mg/kg of propofol) followed by an immediate infusion (equivalent to 1.5 mg/kg/hr of propofol) was also quantified.

For systemic biodistribution, the same dye-doped nanoemulsions (propofol, nicardipine, or doxorubicin-loaded) were administered intravenously as a bolus to Long-Evans rats (N=3). The rats were sacrificed at 24 h post administration to harvest major organs: heart, liver, lungs, kidneys, spleen, and brain. These organs were imaged for IR800 fluorescence (Ex/Em=770/810 nm) using a Lago imaging system and quantified using regions of interest (ROI) of the same size, drawn to be within the image of each organ. The distribution of the nanoemulsion among the organs was calculated by dividing the ROI fluorescence of each tissue by the sum of ROI fluorescence values of all organs.

2.7 Quantifying the plasma concentration of ultrasonically uncaged drug

Under ketamine/xylazine anesthesia, the left femoral vein and tail vein of Long-Evans rats (N=3) was cannulated and then the rat was placed in a supine position and the hair overlying the abdomen was depilated. The ultrasound imaging probe and FUS transducer were placed at "Position 2" (see Fig. 1c). Then, 1 mg/kg drug equivalent nanoemulsion (propofol, doxorubicin, or nicardipine-loaded nanoemulsion) was administered via the tail vein. A 0.25 ml blood sample was taken via the cannulated femoral vein at 2 and 10 mins after intravenous injection. The FUS was then delivered to the lower abdominal aorta from 10 to 14 mins after bolus injection. The FUS conditions were 650 kHz, 50 ms pulses at 1 Hz pulse repetition frequency for 240 pulses (4 min total), with estimated *in situ* peak sonication pressure of 1.5 MPa. A 0.25 ml blood sample was taken at 14.5, 18, 24, 34, and 59 mins after intravenous injection, corresponding to 0.5, 4, 10, 20, and 45 mins after FUS.

A 0.1 ml plasma sample was obtained by a total of 10 min centrifugation at 5,000 g at 4 °C for each blood sample. The drug was then extracted with 0.2 ml organic solvent (hexane for

propofol, and ethyl acetate for nicardipine and doxorubicin). The propofol content in hexane was quantified with fluorescence (Ex/Em= 276/292 nm). For nicardipine, the UV absorbance after extraction into ethyl acetate was measured at 348 nm. For doxorubicin, was measured at 494/595 nm. The drug concentration was calculated using a pre-determined standard curve of drug fluorescence or UV absorbance with respect to drug concentration in the corresponding solvent.

A similar *in vivo* drug uncaging of propofol and nicardipine was also performed by sonication on the brain (i.e. frontal cortex), followed by blood sampling from a cannulated left internal jugular vein. The animals were placed under ketamine/xylazine anesthesia in a stereotactic frame (Image Guided Therapy, Pessac, France) coupled to the FUS system, and immobilized with two ear bars and a bite bar. The FUS transducer was aligned to 7 mm anterior to the interaural line, 2 mm lateral of midline. The blood collection timeline and sonication protocol were similar. The *in situ* peak negative pressure was approximately 1.2 MPa accounting for the attenuation by rat skull.

2.8 Ultra-high-speed optical imaging and passive cavitation detection of nanoemulsions

The ultra-high-speed optical system (illustrated in Fig. 1a) was composed of an inverted microscope (IX70, Olympus, Melville, NY, USA), with a 100x objective and numerical aperture of 1 (Achroplan 100x, Zeiss, Thornwood, NY, USA). Two different particles were tested. First, the nanoemulsions were diluted in saline to approximately 4.5×10^4 nanoparticles (NPs)/μl (counted with a Accusizer 770A, Particle Sizing Systems, Port Richey, FL). Alternatively, in-house made microbubbles (MBs) composed of a gas core containing perfluorobutane (C4F10) encapsulated in a phospholipid shell were prepared as reported previously [25]. The MBs were diluted in saline to approximately 5×10^4 MBs/μl. Each of the diluted solutions was transported through a 200-μm cellulose tube using a manual microinjector (Narishige, Inc., East Meadow, NY, USA). The cellulose tube was placed in a degassed water tank and positioned in the optical field of view of the microscope. A 250-kHz spherically-focused single-element transducer (H115, Sonic Concepts, Bothell, WA, USA) was placed in the degassed water tank and aligned to focus on the cellulose fiber in the microscope's field of view.

The transducer output pressure was calibrated with a wideband needle hydrophone (HNP-0400, ONDA, Sunnyvale, CA, USA), and the received pressure was displayed on a digital oscilloscope (DPO4034, Tektronix, OR, USA). An arbitrary waveform generator (AWG 2021, Tektronix, Wilsonville, OR) was used to generate the desired radio frequency (RF) signal consisting of three-cycles of a sinusoid with a 250 kHz center frequency. The signal was amplified with an RF power amplifier (325LA, ENI, Rochester, NY, USA). Optical images were captured with an ultra-high-speed camera (Imacon 468, DRS Hadland, Santa Cruz, CA, USA). The high-speed camera triggered the arbitrary waveform generator, and after a delay equal to the sound propagation time from the transducer to the cellulose fiber, light from a xenon flash illuminated the microscope's field of view via a 1 mm fiber-optic cable. The ultra-high-speed camera captured a streak image (temporal resolution of 28 ns and spatial resolution of 120 nm) of the diameter of the imaged particle as a function of

time. Post processing of the images was performed in MATLAB (Mathworks, Natick, MA) to yield the resting particle's radius and expansion ratio.

The acoustic spectra of either the nanoemulsion or MB echoes were recorded passively using a flat 1 MHz single element transducer (IMO102HP, Valpey Fisher) during interaction with the 250 kHz pulses. Four independent observations were obtained for each of the particles at a peak negative pressure (PNP) of 500 kPa. The transducer was positioned perpendicular to the 250 kHz transducer in the water tank and aligned azimuthally to focus at the cellulose fiber, as illustrated in Fig. 1b. The manual microinjector was used to introduce the particles into the cellulose fiber, at the same dilutions used in the high-speed camera imaging experiments. The received echoes were displayed using a digital oscilloscope (DPO4034, Tektronix, OR, USA), and saved for post processing in MATLAB. The transmitted pulse consisted of a 150-ms length burst, a peak negative pressure (PNP) of 500 kPa, and a total duration of 2 minutes. The transducer response was calibrated prior to each experiment by introducing degassed saline into the cellulose fiber, recording the spectra following insonation, and subtracting this background signal from the echoes obtained throughout the experiments. Next, each of the particles (NPs or MBs) were injected into the fiber and their corresponding response was recorded.

The NP size before and after ultrasound application were measured using dynamic light scattering (DLS) in a NICOMP™380 ZLS submicron particle analyzer (Particle Sizing System Inc., Santa Barbara, CA, USA). Ultrasound treatment was performed at a center frequency of 270 kHz, a PNP of 800 kPa, and a duration of 2 minutes.

2.9 In vivo uncaging of nicardipine in abdominal aorta

Long-Evans rats (N= 5–6) were positioned in a supine position and the hair overlying the abdomen was removed with electric clippers. The abdominal aorta was imaged to determine the location of the sonication target. Once confirmed, the FUS probe was positioned overlying the target abdominal aorta. Separately, the imaging transducer was positioned over the distal aorta just proximal to the aortic bifurcation (corresponding to Position #1; Fig. 1c). B-mode and power Doppler imaging were performed with a Siemens Acuson S2000 scanner with a Siemens 15L4 transducer using a transmit frequency of 10 MHz for B-mode and 7.5 MHz for power Doppler. For experiments where the probes were reversed (i.e. Position #2; Fig. 1c), the imaging transducer was positioned in the upper abdominal aorta, and the FUS probe was positioned to target the distal aorta. Once the imaging probe and FUS sonication probe were placed, a bolus (~0.3–0.5 ml) of nicardipine-loaded (equivalent to 134 μg/kg nicardipine) or blank nanoemulsions was slowly given through a tail vein catheter. Then, the 650 kHz sonication was initiated at an estimated peak in situ pressure of 1.5 MPa, with pulsed sonication delivered as 50 ms on and 950 ms off (i.e. 1 Hz pulse repetition frequency) for 240 pulses (i.e. 4 min in total). The center frequency of the transducer was 650 KHz (Image Guided Therapy, Pessac, France). At this frequency, with 0.54 dB/cm*MHz of soft tissue attenuation, and typically 7 mm of soft tissue overlying the aorta, we estimate a net attenuation of −0.25 dB, or 3%, of pressure. The aortic distensibility was measured by calculating the percent change in the maximum diameter of the inner aortic wall between the cardiac systole and diastole phases, as shown in the following equation: Aorta distension

%=[(diastolic diameter-systolic diameter)$_{post\text{-}treatment}$/(diastolic diameter-systolic diameter)$_{pre\text{-}treatment}$ - 1]×100%. The treatment in the equation denotes the i.v. injection of nanoparticles or free nicardipine with or without FUS. The measurements were made by two independent observers who were blinded to the experimental condition, and the averaged values were used for analysis.

2.10 Statistical analysis

GraphPad Prism 5 (GraphPad Software, La Jolla, CA, USA) was used for statistical analysis. Comparisons between two groups was performed by two-tailed Student's t test, and that among multiple groups by one-way analysis of variance (ANOVA) with *Tukey's post-hoc* test. A p-value of 0.05 or less was considered statistically different and the *p*-values were categorized as *: $p < 0.05$, **: $p < 0.01$, ***: $p < 0.001$, and ****: $p < 0.0001$.

3. Results

3.1 Moving towards clinical applicability and translation

To enable eventual *in vivo* and clinical applications, we first developed methods for producing polymeric perfluorocarbon nanoemulsions that are scalable and meet clinical standards of sterility (Fig. 2a). We focused on perfluoropentane (PFP) as the choice of perfluorocarbon to optimize between the relatively increased volatility of shorter chain compounds like perfluorobutane and the potential decreased ultrasound responsiveness and higher boiling point of longer chain compounds. Additionally, given that PFP is currently in FDA-approved clinical trials for other applications [26] and has been extensively studied in clinical populations [27], its inclusion would help to lower barriers to eventual translation. We targeted a median Z-average diameter of 400–450 nm, so that a potential expansion during drug uncaging [28] would be unlikely to embolize capillaries. We targeted a median polydispersity index (PDI) of <0.1 to ensure monodispersity of each batch. We found that the PFP content in the reaction significantly affected the particle size, drug loading, monodispersity (Fig. S1), and *in vitro* uncaging efficacy (Fig. S2). We empirically determined that a 2 μl:1 mg ratio of PFP to polymer most reliably met our target size and PDI.

To generate the nanoparticles, the emulsifying polymer and drug were dissolved in tetrahydrofuran (THF), and then sterile phosphate-buffered saline (PBS) was added. The THF was evaporated to completion, leaving drug-loaded polymeric micelles (~30 nm Z-averaged diameter) in saline suspension. Then, PFP was added and the mixture was sonicated in a bath sonicator until the PFP was visibly completely emulsified. Following three cycles of centrifugation and resuspension to remove free drug and polymer, the nanoparticles were filtered twice through a membrane extruder to produce the final suspension. Notably, the shift from immersion sonication, as used previously [22], to bath sonication and membrane extrusion substantially reduced the free drug fraction (4.3% ± 0.9% with the current method vs. 10.8% ± 1.9% with the prior method) and the polydispersity. This shift in production methods also allowed more ease of scaling up of nanoparticle production to dozens of mL with a single sonication, and minimized potential contamination due to exposure to the sonication probe. Dynamic light scattering confirmed

that our current methods produced monodisperse peaks of nanoscale material (Fig. S3). Cryogenic electron microscopy (Cryo-EM) confirmed that the nanoparticles adopted a spherical shape, with a PFP core wrapped with a thin multi-shell structure of polymer of 10–20 nm radially on the surface. Using Cryo-EM, the diameter of the nanoparticles was measured to be 300–400 nm on average, using previously described image analysis protocols (Fig. 2b) [29]. On the surface of nanoparticles, an electron-dense shell (likely consisting of polymer and drug) was observed with multiple density levels, that were lighter than the core density, which likely consisted of PFP. Structural analysis suggests that these shells are stacked radially away from the PFP droplet surface and are likely the hydrophobic drug molecules covered and mixed within the PEG (2kDa)-PLGA (5kDa) chains of the polymer, with an average shell thickness of ~15 nm.

In prior perfluorocarbon nanoemulsion formulations, the particle size, free drug fraction, and polydispersity all increased substantially over the course of hours with incubation either on ice or at room temperature [19,22], and the particles were too unstable to permit a freeze-thaw cycle for long-term storage. To address this instability and significant practical limitation, we used cryoprotectants to enable frozen storage of the particles. The addition of minimal (2.25% w/v) glycerin to the particles had no substantial effect on the physicochemical characteristics and drug loading of the particles (Figs. 2c, S4a,b), yet allowed for improved particle stability (on ice) in terms of physicochemical characteristics in the post-thaw time period (Figs. 2d, S4c,d) and also permitted long-term frozen storage of the particles (Figs. 2e, S4e,f) with stability across multiple freeze-thaw cycles (Fig. S5). This formulation also showed low batch-to-batch variability with no change of physicochemical characteristics across varied particle concentrations (Fig. S4g–i, indexed by the encapsulated drug concentration). With the current protocol, there is a minimal slow increase of the free drug fraction during incubation, rising from ~4% of the initial drug load when fresh to ~8% after 3 hours post-thaw at room temperature (Fig. 2d).

To determine the *in vitro* uncaging efficacy of this novel formulation for ultrasonic drug uncaging, we loaded the particles into thin-walled plastic PCR tubes and then added a layer of organic solvent on top that is immiscible with and of lower density than water (Fig. 2f). Notably, for the organic solvent, we used solvents in which the polymer of these nanoparticles is insoluble, limiting potential disruption of the particles without sonication. Indeed, we observed no evidence of excess free drug elution with simple incubation with the organic solvent in this arrangement. Following focused sonication of the aqueous nanoparticle suspension, the organic layer was collected, and the fluorescence or UV absorbance spectra of this fraction was measured to indicate the amount of drug release. Indeed, there was robust FUS-induced drug release seen with a dose-response relationship with the applied *in situ* peak pressure, and no change of this efficacy between fresh and frozen/thawed nanoparticles, irrespective of the length of time that the particles were frozen (Fig. 2g). Between all the presented experiments, to assess the effect of sonication frequency on uncaging efficacy, a total of three sonication frequencies (270 kHz, 650 kHz, and 1.5 MHz) were used. An inflection point for drug release versus sonication pressure was estimated as 0.2 MPa for 270 kHz sonication (Fig. S7), 0.8 MPa for 650 kHz sonication (Figs. 1g, 3d), and 1.2 MPa for 1.5 MHz sonication (Fig. 3d). The rising inflection point of the pressure needed for drug uncaging with ultrasound frequency may be due to decreased

time for each cycle at the peak positive or negative pressure with higher frequencies. This behavior is usually seen for ultrasound effects that have a mechanical mechanism of action. Notably, the drug uncaging seems to not be associated with inertial cavitation or large amplitude particle oscillation (see Section 3.5). Other processes such as heating or radiation force are unlikely to contribute significantly to the uncaging mechanism, given the decreased efficacy for uncaging with higher sonication frequencies. Drug release also increased with sonication burst length (i.e. time length of sonication pulse), with minimal or no appreciable release with burst lengths below 10 ms and saturation of the effect with burst lengths above 50 ms [23].

To evaluate the suitability of this production protocol for eventual clinical application, we assessed for endotoxin and bacterial contamination using a chromogenic LAL endotoxin assay and growth on LB agar plates, respectively. The endotoxin level measured 0.3 ± 0.05 EU per mg propofol, far lower than 5 EU per mg of active pharmaceutical ingredient (API; propofol in this case, to be used at 1 mg propofol/kg body weight), which is considered to be acceptable for parenteral administration [24], indicating no significant endotoxin contamination. Also, there were no bacteria observed on LB agar plates of the nanoparticle formulation after 72 h at 37 °C, indicating the sterility achievable with this production protocol.

A central hypothesis is that the drug loading and uncaging efficacy of these particles is determined by the interaction between the drug and the hydrophobic domain of the encapsulating diblock-copolymer. To determine the effect of the encapsulating diblock-copolymer on drug loading and uncaging efficacy, we varied the hydrophobic block of the polymer between the common drug delivery polymers of poly-*ε*-caprolactone (PCL), poly-*L*-lactic acid (PLLA), and poly-lactic-co-glycolic acid (PLGA). The molecular weight of these blocks was varied between 2 kDa and 5 kDa. The hydrophilic block of poly-ethylene glycol (PEG; mol. wt. 2 kDa) was kept constant. PLLA particles, particularly with a block molecular weight of 5 kDa, showed increased size and polydispersity, and in many cases developed a precipitate during production (biasing the drug loading estimates), indicating that this polymer was not suitable for these applications (Fig. 3). This may be due to the relatively long crystalline block of PLLA that significantly reduces its solubility in the initial aqueous/organic mixture [30]. PLLA was therefore removed from subsequent studies. There was minimal difference between PCL and PLGA in terms of the resultant particle physicochemical characteristics and drug loading, likely due to the similar hydrophobicity and rigidity of these two materials. Larger hydrophobic blocks yielded greater drug loading (Fig. 3c), with approximately double the drug loading with 5 kDa hydrophobic block sizes compared to 2 kDa. There was a slight difference among the particles in terms of their *in vitro* ultrasonic drug uncaging efficacy (Fig. 3d), with larger hydrophobic blocks trending towards decreased percent uncaging. Given the substantially improved drug loading of 5 kDa vs. 2 kDa hydrophobic blocks relative to this minimally decreased percent uncaging, and the greater reported experience of safety and efficacy in clinical drug delivery applications with PLGA [31,32] compared to PCL, we chose PEG(2 kDa)-PLGA(5 kDa) as the emulsifying polymer of the nanoemulsions for subsequent experiments.

3.2 A generalized platform for targeted drug delivery

To realize the promise of this system as a platform for targeted delivery of a wide variety of drugs, and to estimate the drug features that most enable encapsulation into polymeric perfluoropentane nanoemulsions, we varied the loaded drug across seven molecules: two antihypertensives (calcium channel antagonists verapamil and nicardipine), three anesthetics (propofol, ketamine, and dexmedetomidine), and two chemotherapeutics (doxorubicin and cisplatin). These are all small molecules with molecular weights less than 500 Da and that span the range from hydrophilic (LogP < 0) to hydrophobic molecules (LogP > 0). There was minimal difference of the choice of loaded drug on the particle physicochemical properties (Figs. 4a,b). Instead, there was a strong positive relationship noted between drug hydrophobicity (indicated by LogP, the oil:water partition coefficient) and drug loading (Fig. 4c), with essentially no loading of the hydrophilic compound cisplatin (LogP = −2.2). There were slight differences of *in vitro* ultrasonic drug uncaging efficacy across the different drugs (Fig. 4d), with less hydrophobic agents uncaging more than the most hydrophobic agents as a percent of drug loading; e.g. doxorubicin (LogP = 1.3) had marginally greater drug release versus applied pressure, compared to verapamil or nicardipine (LogP = 3.8). Notably, this trend is reverse to the correlation of LogP and drug loading, consistent with the hypothesis that the drug-nanoparticle binding is determined by the interaction of the drug and the hydrophobic polymer block. These results establish the generalizability of this system for ultrasonic uncaging of hydrophobic drugs.

3.3 In vivo nanoparticle characterization

To determine the clearance kinetics, biodistribution, and biocompatibility of the nanoparticle vehicles in rats, the particles were doped (in addition to the loaded drug) with a dye whose infrared fluorescence is quantitative in blood samples, and which clears from the blood pool within ~5 min in its unincorporated free form. For this analysis, to assess whether the loaded drug affects the biodistribution and clearance of the nanoparticles, we varied the loaded drug between ones with high (nicardipine), intermediate (propofol), and low (doxorubicin) drug loading and correspondingly high, medium, and low LogP. To assess the particle clearance kinetics, the fluorescence for whole blood and plasma samples was quantified after collection at several time points over hours. The plasma fluorescence indicates the rate of generation of drug-loaded micelles as the volatile PFP diffuses out of the nanoparticle core, as well as the potential elution of free dye. Therefore, the difference between the whole-blood and plasma sample fluorescence indicates the nanoparticle blood concentration. There was no substantial effect of the choice of encapsulated drug on particle kinetics or biodistribution (Figs. 5a, c, d). Independent of the particular loaded drug, the particle blood pool concentration followed a dual exponential clearance profile, with half-lives of 10–12 min and 77–97 min for each phase (Fig. S6; Tables 1, S1). Based on this profile, a bolus plus infusion protocol was determined to yield a steady blood particle concentration to enable prolonged usage. Indeed, with this bolus plus infusion protocol, a steady blood particle concentration was seen for over 40 min, with a similar elimination profile to bolus alone following the halt of infusion (Fig. 5b). Independent of the particular loaded drug, the particles showed uptake at 24 h primarily in the liver, followed by spleen and lung, with minimal uptake in kidney and heart, and notably no binding to the brain (Fig. 5e–f). In our experiments, >100 rats have received the current formulation of these particles at these

doses, with some receiving up to nine doses over several weeks, and none has shown visible evidence of toxicity due to particle administration or uncaging. Indeed, no negative change was seen in animal body weight across two weeks of multiple nanoparticle administrations (Fig. 5g). The brains of animals that underwent uncaging in the brain following nanoparticle administration and uncaging sonication showed no evidence of acute injury (e.g. due to cavitation or capillary embolization with nanoparticle expansion) or blood-brain barrier disruption by either histology or contrast-enhanced MRI [28]. These results indicate that, independent of the choice of loaded drugs, these nanoparticles and their uncaging are well tolerated and have clinically practical clearance kinetics to enable acute ultrasonic drug uncaging therapies.

3.4 Quantification of in vivo drug pharmacokinetics with ultrasonic uncaging

Given the favorable clearance kinetics and biodistribution of the nanoparticles, which are each independent of the loaded drug, we then assessed the *in vivo* pharmacokinetics of ultrasound-induced drug release for this system. We first note that no prior *in vivo* demonstration of perfluorocarbon nanoemulsion uncaging, including our own work, demonstrated that this uncaging generally yields a restricted pharmacokinetics or pharmacodistribution of drug release *in vivo*. For this current assay, the plasma concentration of drugs was determined in blood samples taken before and after ultrasound application in rats. In a first scenario, ultrasound was applied to the lower abdominal aorta and blood was sampled from the downstream femoral vein (Fig. 6a–d). In a second scenario, ultrasound was applied to the brain (frontal cortex), similar to our previous implementation of this uncaging [22,23], and blood was sampled from the downstream ipsilateral internal jugular vein (Fig. 6e–f). In each scenario, for each drug, before sonication, there was no significant plasma drug concentration above the limits of detection for this assay. However, following ultrasound (650 kHz, 240 repetitions of 50 ms pulses with 1 Hz pulse repetition frequency, 1.5 MPa estimated peak *in situ* negative pressure for the abdominal aorta or 1.2 MPa estimated peak *in situ* negative pressure for frontal cortex) a sharp rise in plasma drug concentration was noted in the downstream vein, with a subsequent dual-exponential decay profile of the plasma drug concentration. Notably, the pharmacokinetics of the released drug and the estimated dual-exponential decay half-lives (Table S2) were similar whether uncaging was completed in the largest artery of the body (the aorta, Fig. 6a–d) or directly in organ parenchyma where the uncaging would occur in the limited blood volume of the capillary bed (Fig. 6e–f). This indicates that the drug in either case is mostly extracted during a first pass of perfusion, independent of the loaded drug or the sonication site, underlining the specificity and versatility of this drug delivery technique and confirming that ultrasonic drug uncaging from perfluorocarbon nanoemulsions yields pharmacokinetics that are limited in time by ultrasound application.

3.5 These nanoemulsions do not undergo large oscillations or cavitation with sonication

It has been estimated that perfluorocarbon nanoemulsions may undergo a 5–6 fold size expansion and potentially a cavitation-related liquid-to-gas phase transition during sonication [28], raising the risk of vessel embolization or cavitation-induced damage *in vivo*. Additionally, the observation that uncaging efficacy appears to decrease with increasing sonication frequency (Fig. 2g with 650 kHz FUS, Fig. 3d with 1.5 MHz FUS, Fig. S7 with

270 kHz FUS), suggests a mechanical mechanism for the drug uncaging. To better define the physical response of the nanoemulsions to sonication, and given the potential for cavitation to occur with uncaging, both nanoemulsions and microbubbles were optically observed using an ultra-high-speed camera at a rate of 28 ns/frame while being sonicated using a center frequency of 250 kHz, given that cavitation is generally more efficiently induced with lower ultrasound frequencies [33] and therefore increase our sensitivity to detect cavitation. We chose sonication parameters known to induce uncaging with a similar sonication frequency (Fig. S7). Streak images presenting the diameter of the particles as a function of time were captured. Images of ~20 single nanoemulsion particles, and ~20 oscillating microbubbles were captured and processed. Microbubble are known to expand with sonication at a center frequency of 250 kHz [34]. Indeed, with microbubbles, we observed an expansion ratio of 35 at a peak negative pressure (PNP) of 500 kPa (Fig. 7a). Even though this pressure is known to yield effective drug uncaging from these nanoemulsions with 270 kHz sonication (Fig. S7), no observable cavitation or large-amplitude oscillation was observed for these nanoemulsions insonified under similar conditions (Fig. 7b).

The potential cavitation activity induced by a 250 kHz burst for each of the compounds was then estimated using the magnitude of the received echo spectrum recorded passively using a 1 MHz center frequency wide-bandwidth hydrophone (Fig. 7). The acoustic results followed the same trend of the optical observations. The received echo spectrum of the microbubbles indicates strong inertial cavitation under these conditions, with high ultraharmonic components and increased broadband power (black trace, Fig. 7c), whereas harmonic signals of cavitation were not detected with nanoemulsion sonication (red trace, Fig. 7c). The nanoemulsion particle Z-average diameter remained similar before (380.3±126.3 nm) and after FUS (382.8±151.7 nm; Fig. 7d). Considering that decreasing ultrasound frequency increases the likelihood of cavitation and gas body activation [33], since we did not observe cavitation at 250 kHz, with intensities that yield robust drug uncaging (Fig. S7), it is very unlikely that cavitation accompanies drug uncaging with sonication at or around 250 kHz, or at higher frequencies like 650 kHz and 1.5 MHz where cavitation efficiency is reduced. The lack of inertial cavitation or large amplitude oscillations with uncaging suggests low safety risks of this technology for future clinical use, in concordance with our own observations [23].

3.6 Efficacious and localized in vivo ultrasonic drug uncaging

Next, we sought to confirm that these particles retained high therapeutic efficacy *in vivo*. In our previous work, we verified that propofol-loaded perfluorocarbon nanoemulsions could induce drug uncaging that is efficacious enough to silence chemically-induced whole-brain seizures [24] and to yield a localized anesthesia of the brain to map functional connectivity [23]. However, it has remained an open question whether intravascular drug uncaging in high-flow vessels would yield such a restricted pharmacodistribution in space or time (Fig. 6) [23], given the likelihood for intra-arterial uncaging to spread the drug throughout the downstream body.

Given that drug uncaging with this technique occurs intravascularly, we note that the broadest pharmacodistribution would occur with uncaging directed to an artery that subtends

a large region of the body, especially for a drug that mainly acts on the vessel itself, instead of in a target organ. Notably, vasodilating agents such as nicardipine and verapamil are used clinically to relieve arterial spasm as seen with cerebral vasospasm and other conditions [35], by relaxing the smooth muscle of the vessel wall. For example, nicardipine has been shown to relax the wall of the aorta and increase its distensibility in humans [25]. While effective, these agents have undesirable side effects of generalized hypotension when given systemically, due to decreasing the systemic vascular resistance by action beyond the target vessel. This hypotension can result in end organ infarction in severe cases. In order to minimize this effect, the vasodilator must be infused via an invasive intra-arterial catheter placed within the target vessel or immediately upstream. For ultrasonic vasodilator uncaging to achieve similarly localized effects, the vasodilator must bind the arterial smooth muscle immediately after ultrasound-induced release from the nanoparticles, given that arterial velocities are generally on the order of 0.3–0.5 m/s [37] and given the relatively slow clearance of nicardipine compared to shorter-acting agents like propofol (Fig. 6). Therefore, to stress-test whether ultrasonic drug uncaging from perfluorocarbon nanoemulsions could achieve a local and substantial drug effect, and to determine the effective locality of intra-arterial infusion using this method, we assessed whether ultrasonic nicardipine uncaging could yield a localized change in vessel wall compliance of the rat abdominal aorta (~7 cm in length, ~1 mm luminal diameter), the highest flow vessel of the body. With ultrasonic nicardipine uncaging in the aorta upstream of an ultrasound imaging probe, a substantial difference in systolic and diastolic aortic diameters was indeed noted compared to the pre-uncaging baseline (Fig. 8; Videos S1–2). This effect was not seen with ultrasound alone, with nanoparticle administration alone, with ultrasound applied to blank nanoparticles, or with nicardipine uncaging applied downstream of the imaging probe (‘Position 2’ in Fig. 1c; Fig. 8b), confirming that this effect is specific to nicardipine uncaging of the proximal aorta. In fact, compared with a systemic bolus of free nicardipine that is matched in terms of the total nicardipine dose, ultrasonically uncaged nicardipine had a more potent effect on the vessel wall distensibility (Fig. 8b), even though it is likely that only a minority of the nanoparticles were exposed to the sonication field. Furthermore, systemic nicardipine administration increased the aortic blood velocity by 41% on average (Fig. S8), due to a decrease in systemic vascular resistance with peripheral nicardipine action that corresponds to its antihypertensive action. Similarly, uncaging of nicardipine nanoparticles in the distal aorta (i.e. ‘Position 2’) increased the blood flow velocity in the aorta (Fig. S8), likely by relaxing the arterial/arteriolar smooth muscle in the lower limbs and therefore decreasing the vascular resistance seen by the lower aortic blood flow. However, importantly, this effect was not seen with ultrasonic nicardipine uncaging in the proximal aorta (‘Position 1’), confirming that ultrasonic drug uncaging is limited to effects in the immediate region of sonication, given the length of the rat aorta (~7 cm) and the rapid speed of rat aortic flows (~0.3–0.5 m/s; Fig. S8) [38]. This confirms that ultrasonic drug uncaging yields a volume of distribution of the drug that is effectively confined to the sonicated region, which in turn results in an effective amplification of the local drug concentration and effect relative to systemic free drug administration. Furthermore, these results demonstrate that this localized drug-receptor binding can occur even in the presence of rapid aortic flows. Notably, the majority of this effect occurred with the first minute of sonication (Fig. 8c), confirming the rapid temporal kinetics of the bioeffects of ultrasonic drug uncaging (Fig. 6).

4. Discussion

We have shown that polymeric perfluorocarbon nanoemulsions are a versatile platform for ultrasonic drug uncaging, with a ready path for clinical translation. We have described scalable production methods that hew to clinical standards of sterility and produce particles that are stable for both long-term frozen storage and for hours of use after thawing, as well as for multiple freeze-thaw cycles (Figs. 2, S1–S2, S4–S5). We have confirmed that longer hydrophobic blocks of the emulsifying polymers yield greater drug loading, with minimal effect of the specific choice of polymer on drug uncaging efficacy (Fig. 3). We further explicitly demonstrate the ability of this technology to encapsulate and selectively uncage drugs that span a range of hydrophobicity, drug classes, and receptor binding profiles (Fig. 4). Indeed, while drug loading increases and drug uncaging minimally decreases with drug hydrophobicity, all other features of the particles, including their drug release efficacy, clearance kinetics, and biodistribution are relatively independent of the particular drug that is encapsulated (Figs. 4, 5, S6; Tables 1, S1). Additionally, *in vivo* ultrasonic drug uncaging with these particles produces a restricted pharmacokinetics (Figs. 6; Table S2) and a localized pharmacodistribution following intravascular release of the drug cargo (Figs. 8, S7, Videos S1–2), without evidence of significant expansion or observable cavitation during sonication (Fig. 7), indicating low risk of adverse effects on the surrounding tissue upon drug uncaging. Indeed, the frequency dependence of uncaging efficacy (Figs. 2–4, S7) suggests a mechanical mechanism of ultrasonic uncaging, without significant contribution from heating or radiation force-type mechanisms. Notably, no significant adverse events have been observed with administering these nanoparticles at these doses, or with uncaging itself, in these experiments (e.g. Fig. 5g) or our other recent experiments [23]. Indeed, >100 rats have now undergone ultrasonic drug uncaging in our hands, without clear evidence of an adverse response. Combined with our prior results showing efficacy of this system for application in the brain [22,23], these results indicate that ultrasonic drug uncaging with perfluorocarbon nanoemulsions provides a noninvasive and wireless analogue to catheter-based intravascular infusion of hydrophobic drugs, with maximal on-target drug uncaging and minimal off-target systemic side effects.

There are numerous potential applications for ultrasonic drug uncaging. In the brain, focal uncaging of neuromodulatory agents could allow pharmacological adjuncts to psychiatric therapy sessions that are tailored to the particular neural circuit pathophysiology for a given patient [39]. This technology could also allow pharmacological mapping of neural circuits [23] to better target more permanent interventions such as surgical resection, ablation, or deep-brain stimulation. Additionally, current therapy for vessel spasm disorders, such as the cerebral vasospasm that unfortunately accompanies many cases of subarachnoid hemorrhage [35] is difficult given that the agents that best relieve the spasm also act systemically as potent anti-hypertensives. The noninvasive local relaxation of the walls of the affected vessels, as modeled in Fig. 8, would be beneficial as a noninvasive alternative to current catheter-based intra-arterial vasodilator infusions, especially as this nanotechnology apparently achieves local vasodilatation without concomitant loss of systemic vascular resistance (Fig. S8) and therefore without systemic hypotension. Finally, many chemotherapeutics are known to be effective for treatment of a given tumor cell type, yet

cannot be administered in effective doses systemically due to intolerable side effects in the rest of the body. Ultrasonic chemotherapeutic uncaging within the tumor and its immediate margin would therefore be of utility.

Future work with this technology will move ultrasonic drug uncaging to clinical practice, first by validating this approach in large animal models, and then by beginning first-in-human trials to establish the safety and the efficacy of drug uncaging with this technique. Importantly, the constituent components of these nanoparticles – namely the drugs under consideration, PEG, PLGA [31], and PFP [26,27] – have each been used in clinical trials with excellent safety profiles, lowering the barrier to translation for these nanoparticles. Additional future work will focus on expanding this technology to include encapsulation of hydrophilic small molecules, as well as larger macromolecules like peptides, antibody fragments, and nucleic acids. Given their potential for clinical translation, their ability to uncage a variety of important hydrophobic drugs, and the potent local pharmacological bioeffects they can induce in the brain and in the body, polymeric perfluoropentane nanoemulsions are poised to have significant impact both for clinical care as well as our scientific understanding of how pharmaceuticals mediate their bioeffects.

5. Conclusions

We have developed polymeric perfluoropentane nanoemulsions as a versatile platform for targeted drug delivery that is primed for clinical translation. These nanoparticles are produced with clinically-translatable production methods and have stability, drug loading, and drug release efficacy that is suitable for clinical application. This system efficaciously encapsulates and ultrasonically uncages a wide variety of drugs, with drug loading increasing with hydrophobicity, and with essentially all other features of the particles being independent of the particular encapsulated drug. The *in vivo* pharmacokinetics and pharmacodistribution of drug release with this technology is defined by when and where ultrasound is applied. Importantly, there is no evidence of cavitation or significant particle expansion during sonication, suggesting minimal risk of cavitation-induced injury or vascular embolization with this technique. In this manner, polymeric perfluorocarbon nanoemulsions can potentially be used for wireless intravascular infusions of hydrophobic drugs, as noninvasive analogues of current catheter-based therapies.

Supplementary Material

Refer to Web version on PubMed Central for supplementary material.

Acknowledgements

This work was funded with grant support from the National Institutes of Health (BRAIN Initiative RF1 MH114252), the National Cancer Institute/Stanford Center for Cancer Nanotechnology Excellence (NIH U54 CA199075), the Dana Foundation, the Foundation of the American Society for Neuroradiology, and the Wallace H. Coulter Foundation. We would also like to thank William T. Newsome, PhD and the Stanford Neurosciences Institute for additional funding support. We would like to thank Yun-Sheng Chen, PhD for assistance in the design and preparation of the nanoemulsions, and Marko Jakovljevic, PhD and Jeremy Dahl, PhD for access to and training on the Siemens Acuson S2000 scanner. We would like to thank Kim Butts Pauly, PhD, Jennifer Dionne, PhD, and the whole Airan Lab for helpful discussions.

Abbreviations

FUS	focused ultrasound
PFP	perfluoropentane
PEG	polyethylene glycol
PLGA	poly(*D,L* lactic-co-glycolic acid) di-block copolymer
PCL	poly-ε-caprolactone
PLLA	poly-*L*-lactide
LAL	Limulus, Amebocyte Lysate
PDI	polydispersity
MRI	magnetic resonance imaging
i.v.	intravenous
MB	microbubble

References

[1]. Imai N, Ishigami M, Ishizu Y, Kuzuya T, Honda T, Hayashi K, Hirooka Y, Goto H, Transarterial chemoembolization for hepatocellular carcinoma: A review of techniques, World Journal of Hepatology. 6 (2014) 844–850. doi:10.4254/wjh.v6.i12.844. [PubMed: 25544871]

[2]. Baxendale S, The Wada test., Current Opinion in Neurology. 22 (2009) 185–9. doi:10.1097/WCO.0b013e328328f32e. [PubMed: 19289955]

[3]. Bederson JB, Connolly ES, Batjer HH, Dacey RG, Dion JE, Diringer MN, Duldner JE, Harbaugh RE, Patel AB, Rosenwasser RH, Guidelines for the Management of Aneurysmal Subarachnoid Hemorrhage, Stroke. 40 (2009) 994LP–1025. [PubMed: 19164800]

[4]. Haga Y, Esashi M, Biomedical microsystems for minimally invasive diagnosis and treatment, Proceedings of the IEEE. 92 (2004) 98–114. doi:10.1109/JPROC.2003.820545.

[5]. Tong R, Chiang HH, Kohane DS, Photoswitchable nanoparticles for in vivo cancer chemotherapy, Proceedings of the National Academy of Sciences. 110 (2013) 19048–19053. doi:10.1073/pnas.1315336110.

[6]. Wei J-P, Chen X-L, Wang X-Y, Li J-C, Shi S-G, Liu G, Zheng N-F, Polyethylene glycol phospholipids encapsulated silicon 2,3-naphthalocyanine dihydroxide nanoparticles (SiNcOH-DSPE-PEG(NH2) NPs) for single NIR laser induced cancer combination therapy, Chinese Chemical Letters. 28 (2017) 1290–1299. doi:10.1016/j.cclet.2017.01.007.

[7]. Xu C, Chen F, Valdovinos HF, Jiang D, Goel S, Yu B, Sun H, Barnhart TE, Moon JJ, Cai W, Bacteria-like mesoporous silica-coated gold nanorods for positron emission tomography and photoacoustic imaging-guided chemo-photothermal combined therapy, Biomaterials. 165 (2018) 56–65. doi:10.1016/j.biomaterials.2018.02.043. [PubMed: 29501970]

[8]. Baghirov H, Snipstad S, Sulheim E, Berg S, Hansen R, Thorsen F, Mørch Y, de Davies CL, Åslund AKO, Ultrasound-mediated delivery and distribution of polymeric nanoparticles in the normal brain parenchyma of a metastatic brain tumour model, PLOS ONE. 13 (2018) e0191102. doi:10.1371/journal.pone.0191102. [PubMed: 29338016]

[9]. Rapoport N, Drug-Loaded Perfluorocarbon Nanodroplets for Ultrasound-Mediated Drug Delivery, Advances in Experimental Medicine and Biology. 880 (2016) 221–41. doi:10.1007/978-3-319-22536-4_13. [PubMed: 26486341]

[10]. Yang K, Hu L, Ma X, Ye S, Cheng L, Shi X, Li C, Li Y, Liu Z, Multimodal Imaging Guided Photothermal Therapy using Functionalized Graphene Nanosheets Anchored with Magnetic Nanoparticles, Advanced Materials. 24 (2012) 1868–1872. doi:10.1002/adma.201104964. [PubMed: 22378564]

[11]. Wu M, Huang S, Magnetic nanoparticles in cancer diagnosis, drug delivery and treatment (Review), Molecular and Clinical Oncology. 7 (2017) 738–746. doi:10.3892/mco.2017.1399. [PubMed: 29075487]

[12]. Kim Y, Advances in MR image-guided high-intensity focused ultrasound therapy, International Journal of Hyperthermia. 31 (2015) 225–232. doi:10.3109/02656736.2014.976773. [PubMed: 25373687]

[13]. Hossann M, Kneidl B, Peller M, Lindner L, Winter G, Thermosensitive liposomal drug delivery systems: state of the art review, International Journal of Nanomedicine. 9 (2014) 4387. doi: 10.2147/IJN.S49297. [PubMed: 25258529]

[14]. Dunne M, Hynynen K, Allen C, Thermosensitive nanomedicines could revolutionize thermal therapy in oncology, Nano Today. 16 (2017) 9–13. doi:10.1016/j.nantod.2017.08.001.

[15]. Rwei AY, Paris JL, Wang B, Wang W, Axon CD, Vallet-Regí M, Langer R, Kohane DS, Ultrasound-triggered local anaesthesia, Nature Biomedical Engineering. 1 (2017) 644–653. doi: 10.1038/s41551-017-0117-6.

[16]. Duncanson WJ, Arriaga LR, Ung WL, Kopechek JA, Porter TM, Weitz DA, Microfluidic Fabrication of Perfluorohexane-Shelled Double Emulsions for Controlled Loading and Acoustic-Triggered Release of Hydrophilic Agents, Langmuir. 30 (2014) 13765–13770. doi:10.1021/la502473w. [PubMed: 25340527]

[17]. Zhang J, Wang S, Deng Z, Li L, Tan G, Liu X, Zheng H, Yan F, Ultrasound-Triggered Drug Delivery for Breast Tumor Therapy Through iRGD-Targeted Paclitaxel-Loaded Liposome-Microbubble Complexes, (2018). doi:10.1166/jbn.2018.2594.

[18]. Dou Y, Hynynen K, Allen C, To heat or not to heat: Challenges with clinical translation of thermosensitive liposomes, Journal of Controlled Release. 249 (2017) 63–73. doi:10.1016/J.JCONREL.2017.01.025. [PubMed: 28122204]

[19]. Rapoport N, Nam K-H, Gupta R, Gao Z, Mohan P, Payne A, Todd N, Liu X, Kim T, Shea J, Scaife C, Parker DL, Jeong E-K, Kennedy AM, Ultrasound-mediated tumor imaging and nanotherapy using drug loaded, block copolymer stabilized perfluorocarbon nanoemulsions, Journal of Controlled Release. 153 (2011) 4–15. doi:10.1016/j.jconrel.2011.01.022. [PubMed: 21277919]

[20]. Rapoport N, Gao Z, Kennedy A, Multifunctional Nanoparticles for Combining Ultrasonic Tumor Imaging and Targeted Chemotherapy, J Natl Cancer Inst. 99 (2007) 1095–1106. doi:10.1093/jnci/djm043. [PubMed: 17623798]

[21]. Li N, Xu F, Cheng J, Zhang Y, Huang G, Zhu J, Shen X, He D, Perfluorocarbon Nanocapsules Improve Hypoxic Microenvironment for the Tumor Ultrasound Diagnosis and Photodynamic Therapy, (2018). doi:10.1166/jbn.2018.2656.

[22]. Airan RD, Meyer RA, Ellens NPK, Rhodes KR, Farahani K, Pomper MG, Kadam SD, Green JJ, Noninvasive Targeted Transcranial Neuromodulation via Focused Ultrasound Gated Drug Release from Nanoemulsions, Nano Letters. 17 (2017) 652–659. doi:10.1021/acs.nanolett.6b03517. [PubMed: 28094959]

[23]. Wang JB, Aryal M, Zhong Q, Vyas DB, Airan RD, Noninvasive Ultrasonic Drug Uncaging Maps WholeBrain Functional Networks, Neuron. (2018). doi:10.1016/j.neuron.2018.10.042.

[24]. O. of R.A. FDA, Inspection Technical Guides - Bacterial Endotoxins/Pyrogens, (n.d.). https://www.fda.gov/iceci/inspections/inspectionguides/inspectiontechnicalguides/ucm072918.htm (accessed August 27, 2018).

[25]. Zhang H, Tam S, Ingham ES, Mahakian LM, Lai C-Y, Tumbale SK, Teesalu T, Hubbard NE, Borowsky AD, Ferrara KW, Ultrasound molecular imaging of tumor angiogenesis with a neuropilin-1-targeted microbubble, Biomaterials. 56 (2015) 104–113. doi:10.1016/j.biomaterials.2015.03.043. [PubMed: 25934284]

[26]. University of Arkansas, A Phase 1b in Patients With Acute Ischemic Stroke - Full Text View - ClinicalTrials.gov, ClinicalTrials.Gov. (2016). https://clinicaltrials.gov/ct2/show/study/NCT02963376 (accessed April 2, 2018).

[27]. Correas J-M, Meuter AR, Singlas E, Kessler DR, Worah D, Quay SC, Human pharmacokinetics of a perfluorocarbon ultrasound contrast agent evaluated with gas chromatography, Ultrasound in Medicine & Biology. 27 (2001) 565–570. doi:10.1016/S0301-5629(00)00363-X. [PubMed: 11368867]

[28]. Sheeran PS, Dayton PA, Phase-Change Contrast Agents for Imaging and Therapy, Current Pharmaceutical Design. 18 (2012) 2152–2165. doi:10.2174/138161212800099883. [PubMed: 22352770]

[29]. Kheirolomoom A, Mahakian LM, Lai C-Y, Lindfors HA, Seo JW, Paoli EE, Watson KD, Haynam EM, Ingham ES, Xing L, Cheng RH, Borowsky AD, Cardiff RD, Ferrara KW, Copper −Doxorubicin as a Nanoparticle Cargo Retains Efficacy with Minimal Toxicity, Mol. Pharmaceutics 7 (2010) 1948–1958. doi:10.1021/mp100245u.

[30]. Gupta R, Shea J, Scaife C, Shurlygina A, Rapoport N, Polymeric micelles and nanoemulsions as drug carriers: Therapeutic efficacy, toxicity, and drug resistance, Journal of Controlled Release. 212 (2015) 70–77. doi:10.1016/j.jconrel.2015.06.019. [PubMed: 26091919]

[31]. Makadia HK, Siegel SJ, Poly Lactic-co-Glycolic Acid (PLGA) as Biodegradable Controlled Drug Delivery Carrier., Polymers. 3 (2011) 1377–1397. doi:10.3390/polym3031377. [PubMed: 22577513]

[32]. Senapati S, Mahanta AK, Kumar S, Maiti P, Controlled drug delivery vehicles for cancer treatment and their performance, Signal Transduction and Targeted Therapy. 3 (2018). doi:10.1038/s41392-017-0004-3.

[33]. Yang X, Jo J, Enhanced cavitation by using two consecutive ultrasound waves at different frequencies, Appl Phys Lett. 105 (2014). doi:10.1063/1.4902118.

[34]. Ilovitsh T, Ilovitsh A, Foiret J, Caskey CF, Kusunose J, Fite BZ, Zhang H, Mahakian LM, Tam S, Butts-Pauly K, Qin S, Ferrara KW, Enhanced microbubble contrast agent oscillation following 250 kHz insonation, Scientific Reports. 8 (2018) 16347. doi:10.1038/s41598-018-34494-5. [PubMed: 30397280]

[35]. Kumar G, Shahripour RB, Harrigan MR, Vasospasm on transcranial Doppler is predictive of delayed cerebral ischemia in aneurysmal subarachnoid hemorrhage: a systematic review and meta-analysis, Journal of Neurosurgery. 124 (2016) 1257–1264. doi:10.3171/2015.4.JNS15428. [PubMed: 26495942]

[36]. Honda T, Hamada M, Shigematsu Y, Matsumoto Y, Matsuoka H, Hiwada K, Effect of antihypertensive therapy on aortic distensibility in patients with essential hypertension: comparison with trichlormethiazide, nicardipine and alacepril., Cardiovascular Drugs and Therapy. 13 (1999) 339–46. [PubMed: 10516870]

[37]. Benessiano J, Levy BI, Michel J-B, Instantaneous aortic blood flow measurement with range-gated doppler flowmeter in anesthetized rat, Journal of Pharmacological Methods. 14 (1985) 99–110. doi:10.1016/0160-5402(85)90047-6. [PubMed: 3162065]

[38]. Park H, Yeom E, Lee SJ, X-ray PIV measurement of blood flow in deep vessels of a rat: An *in vivo* feasibility study, Scientific Reports. 6 (2016) 19194. doi:10.1038/srep19194. [PubMed: 26777719]

[39]. Airan R, Neuromodulation with nanoparticles, Science (New York, N.Y.). 357 (2017) 465. doi:10.1126/science.aao1200.

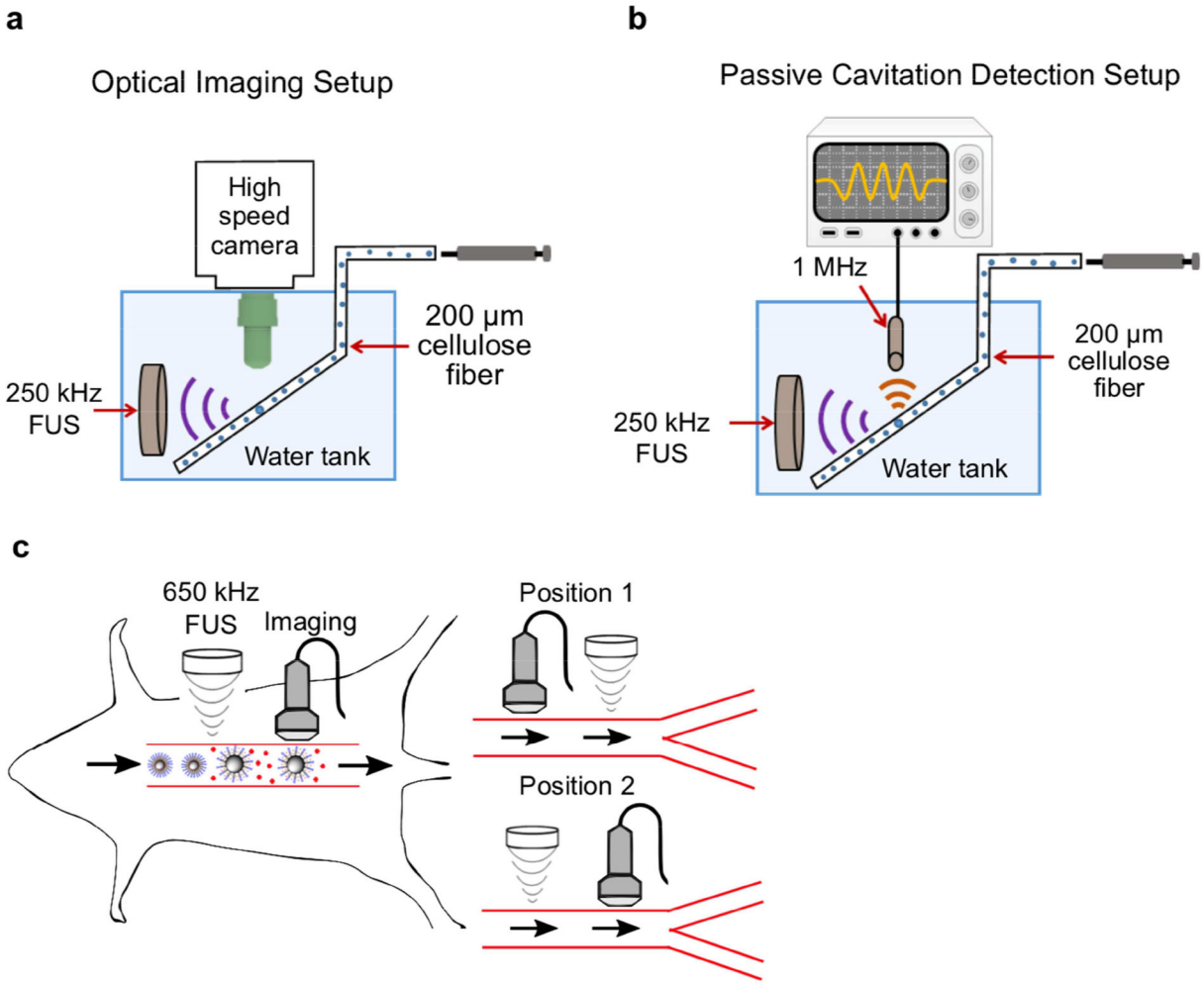

Fig. 1.

Experimental setup of **(a)** ultra-high-speed optical imaging and **(b)** passive cavitation detection of polymeric PFP nanoemulsions. **(c)** Experimental schematic for assaying the effect of *in vivo* ultrasonic nicardipine uncaging from nanoparticles on rat aortic wall compliance. Uncaging is applied to the aorta either upstream (Position 1) or downstream (Position 2) of imaging.

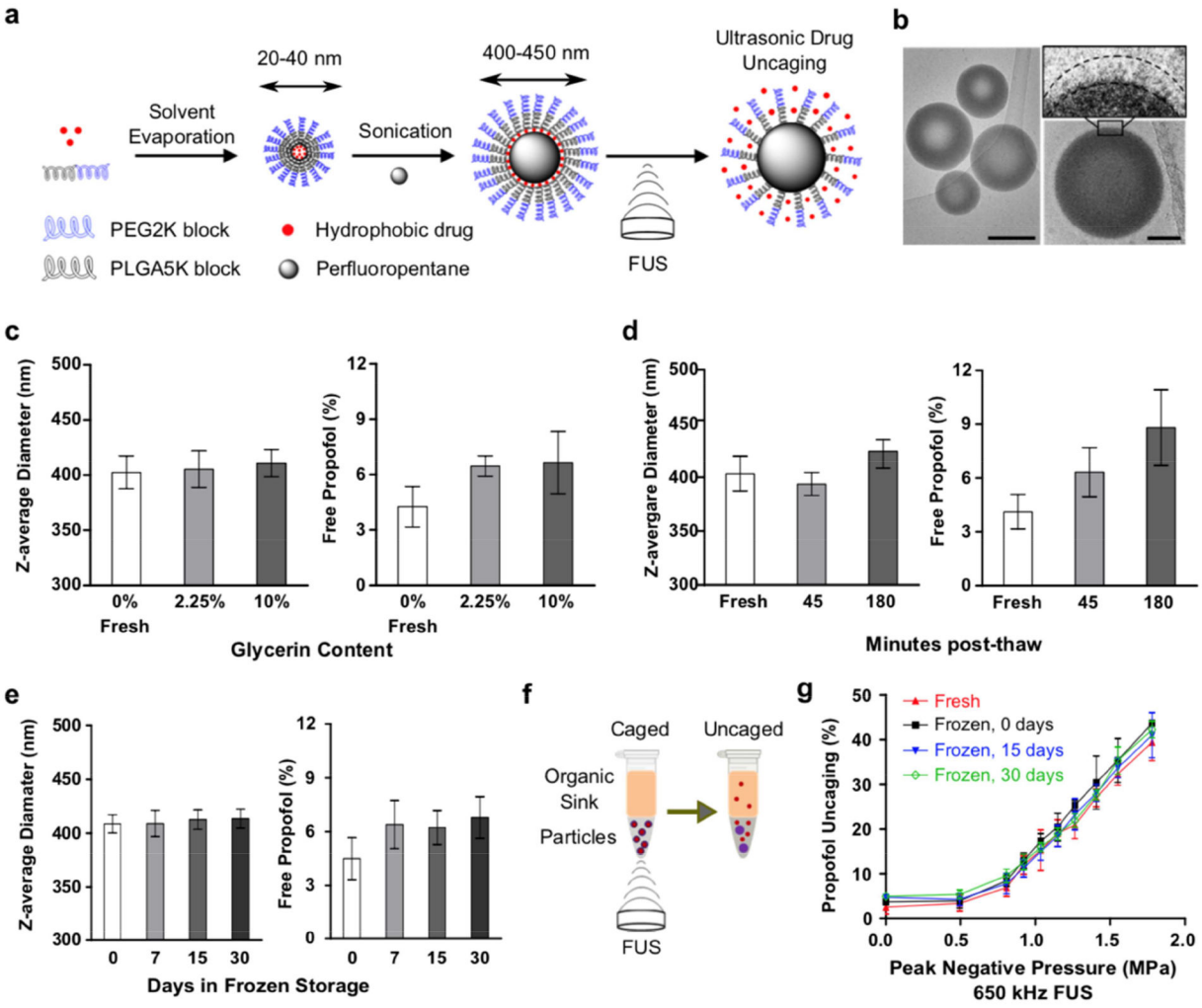

Fig. 2. Nanoparticle production optimized for stability and efficacy *in vitro*.

(a) Schematic of nanoparticle production and ultrasonic drug uncaging. **(b)** Representative Cryo-EM images of spherical nanoparticles (left column; scale bar: 200 nm) and a magnified single nanoparticle observed with a thin layer of polymer on the surface of the PFP droplet (right column; scale bar: 50 nm). The surface densities are likely the hydrophobic drug and PLGA (5kDa)-PEG (2kDa) chains. **(c-e)** Glycerin serves as a cryoprotectant to improve nanoparticle stability through frozen storage and thawing, compared to fresh ("0 days", "0% glycerin") nanoparticle production. **(f)** Experimental schematic to assay ultrasonic drug uncaging efficacy *in vitro*. **(g)** Intact ultrasonic drug uncaging efficacy *in vitro* (650 kHz sonication, 60 repetitions of alternating 50 ms pulses and 950 ms pauses at 1 Hz pulse repetition frequency) for frozen & thawed nanoparticles compared to fresh. Mean +/− S.D. are presented for groups of N=3. ***: $p < 0.001$ by two-tailed t-test.

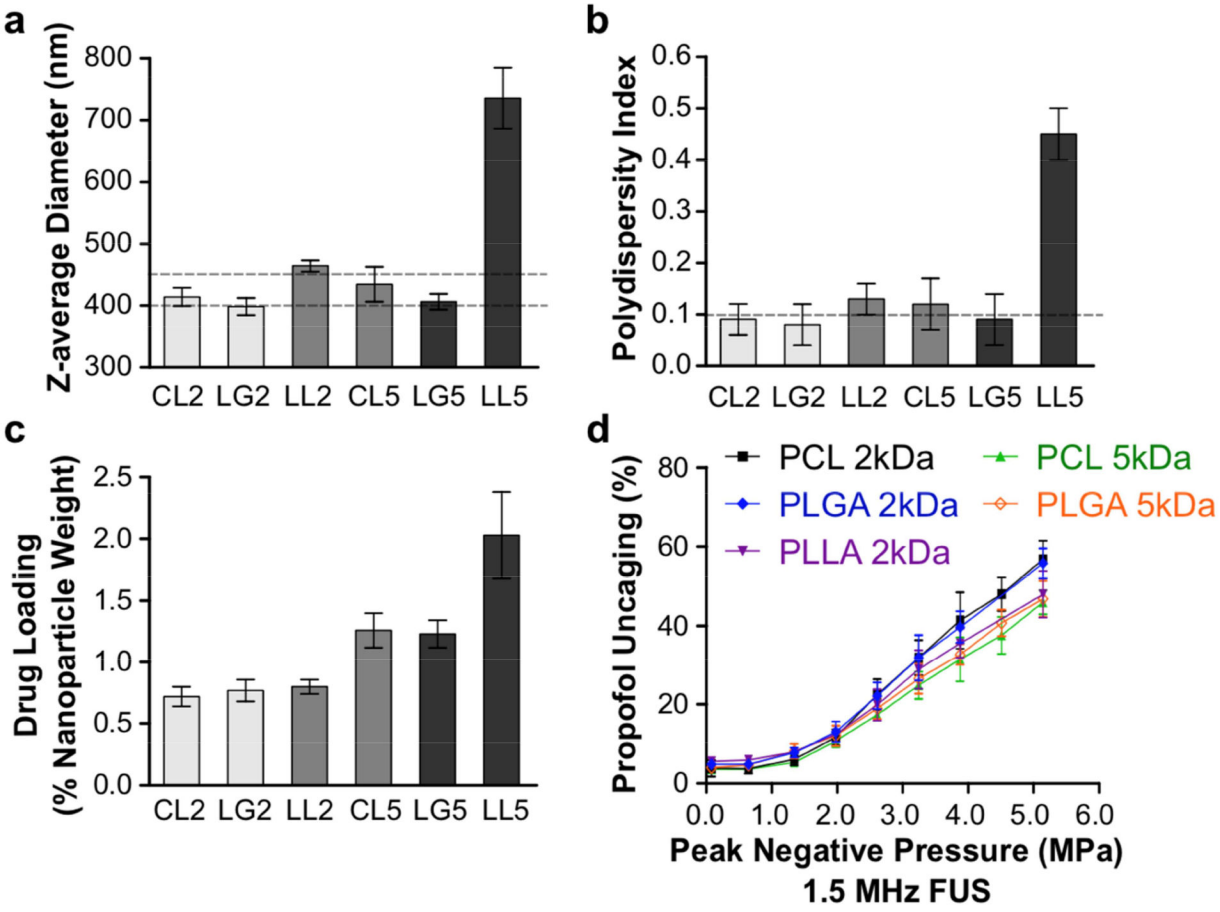

Fig. 3. Variation of physicochemical properties and drug release with choice of emulsifying polymer for drug-loaded perfluoropentane nanoemulsions.

Diblock-copolymers were tested consisting of a hydrophilic block of PEG (2 kDa) and a choice of hydrophobic block among: PCL (2 kDa, CL2, or 5 kDa, CL5), PLGA (2 kDa, LG2, or 5 kDa, LG5), or PLLA (2 kDa, LL2, or 5 kDa, LL5) **(a)** Z-average diameter (dashed lines at the target of 400–450 nm), **(b)** polydispersity index (dashed line at target of 0.1), **(c)** propofol drug loading, and **(d)** ultrasonic propofol uncaging *in vitro* (1.5 MHz sonication, 60 repeats of alternating 50 ms pulses and 950 ms pauses at 1 Hz pulse repetition frequency) was quantified. Mean +/− S.D. are presented for groups of N=3.

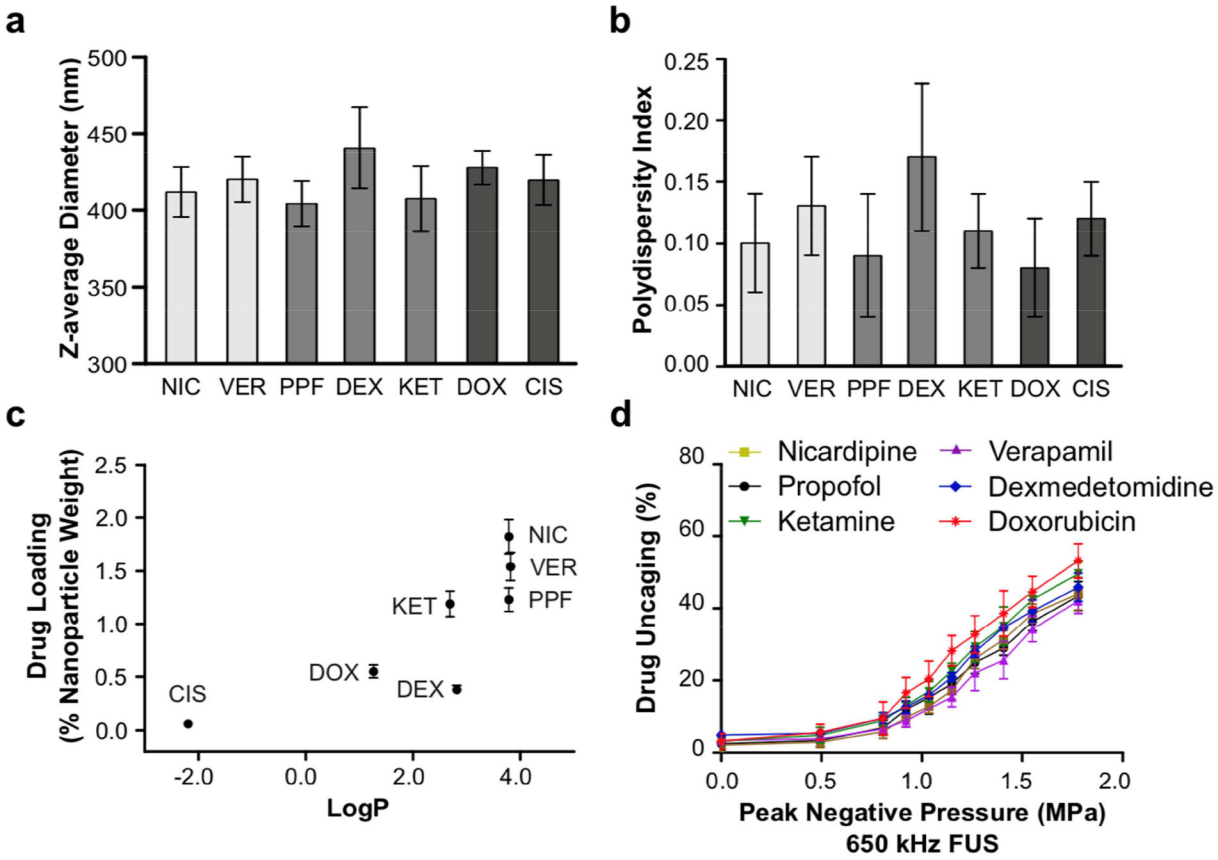

Fig. 4. Polymeric perfluoropentane nanoemulsions are a platform for ultrasonic uncaging of hydrophobic drugs.

(a) Z-average diameter, **(b)** polydispersity index, **(c)** drug loading, and **(d)** ultrasonic drug uncaging *in vitro* (650 kHz sonication, 60 repetitions of 50 ms pulses and 950 ms pauses at 1 Hz pulse repetition frequency) of PEG(2 kDa)-PLGA(5 kDa) perfluoropentane nanoemulsions loaded with propofol (PPF), nicardipine (NIC), verapamil (VER), dexmedetomidine (DEX), ketamine (KET), doxorubicin (DOX), or cisplatin (CIS). Mean +/− S.D. are presented for groups of N=3. Cisplatin-loaded nanoparticles were not tested for *in vitro* uncaging due to low drug loading. In the bar charts, drugs of a similar pharmacologic class (vasodilators, anesthetics, chemotherapeutics) are grouped.

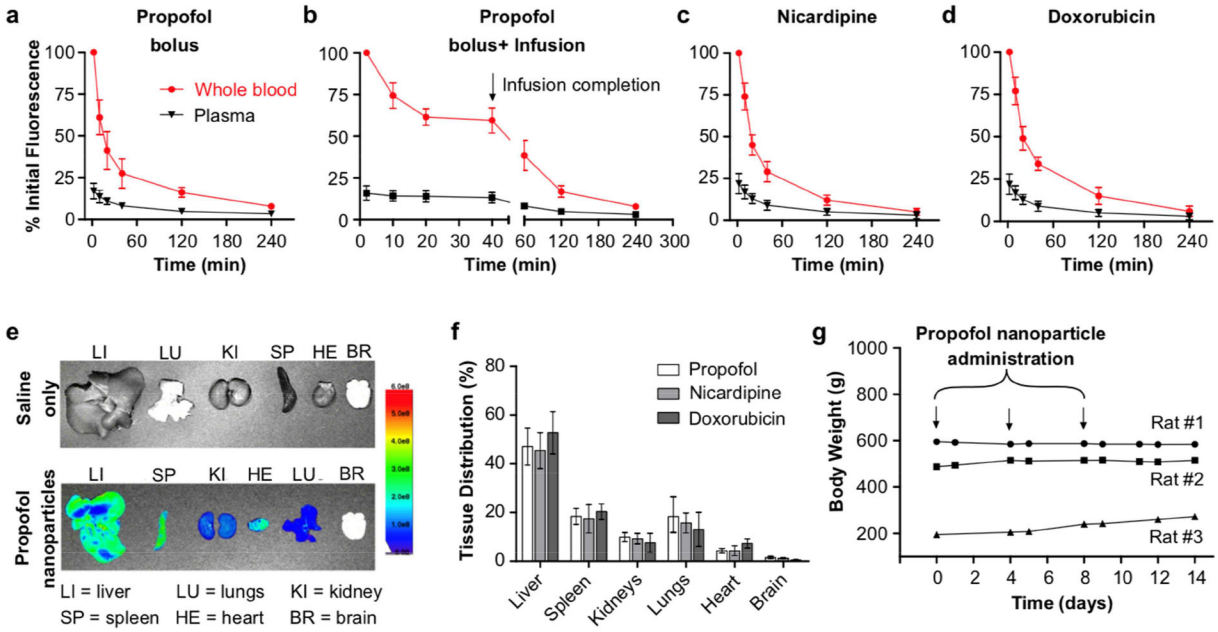

Fig. 5. Nanoemulsions are well-tolerated in rats with practical nanoparticle clearance kinetics and biodistribution that is independent of the loaded drug.

Particle kinetics after intravenous administration of **(a)** propofol-loaded nanoparticles as a bolus (1 mg/kg encapsulated propofol), **(b)** propofol-loaded nanoparticles as an i.v. infusion (bolus of 1 mg/kg + infusion of 1.5 mg/kg/hr encapsulated propofol), **(c)** nicardipine-loaded nanoparticles as a bolus (1 mg/kg encapsulated nicardipine), and **(d)** doxorubicin-loaded nanoparticles as a bolus (1 mg/kg encapsulated doxorubicin). **(e)** Sample images of IR dye fluorescence in organs harvested 24 h after saline (top) and nanoparticle (bottom) administration to rats. **(f)** Tissue distribution of propofol, nicardipine, or doxorubicin-loaded nanoparticles 24 h after i.v. bolus (1 mg/kg encapsulated drug). **(g)** Body weight of rats administered 3 boluses of propofol-loaded nanoparticles over 8 days. On Day 0, Rat #1: 15 weeks old and body weight 595 g; Rat #2: 11 weeks old and body weight 457 g; Rat#3: 5 weeks old and body weight 195 g. Mean +/−S.D. are presented for groups of N=3.

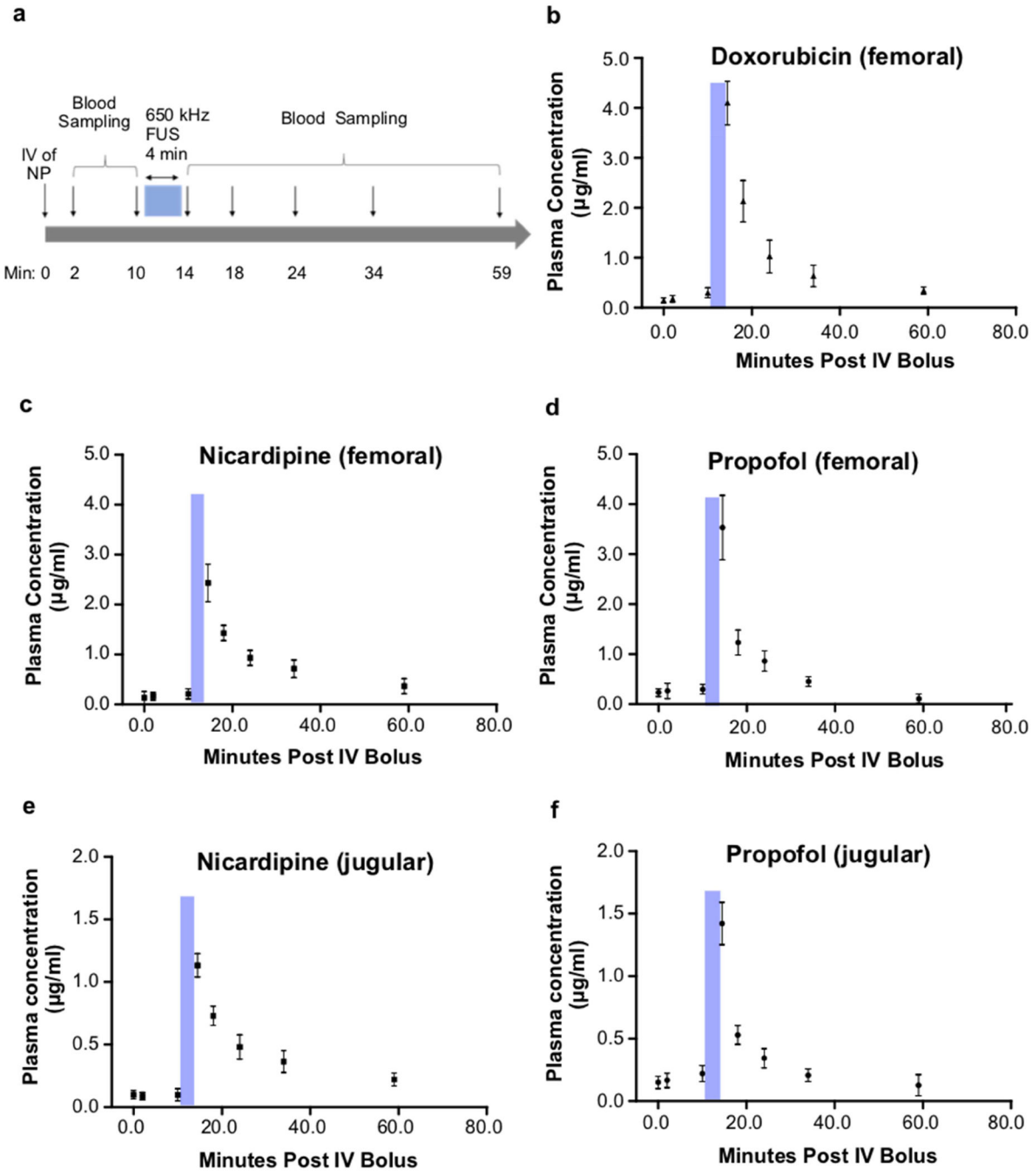

Fig. 6. Drug pharmacokinetics following ultrasonic drug uncaging.

(a) Experimental timeline of blood sampling before and after FUS (650 kHz, 240 repetitions of 50 ms pulses with 950 ms pauses, 1 Hz pulse repetition frequency, estimated *in situ* peak pressure of 1.5 MPa for femoral sampling, 1.2 MPa for jugular sampling). **(b-d)** Plasma drug profile following sonication of the lower abdominal aorta and blood sampling of the left femoral vein. **(e-f)** Plasma drug profile following sonication of the brain frontal cortex and blood sampling of the ipsilateral internal jugular vein. Blue bars indicate FUS timing.

Samples at t=0 min were taken immediately prior to nanoparticle infusion via a tail vein and represent the assay sensitivity limits. Presented are mean +/− S.D. for groups of N=3.

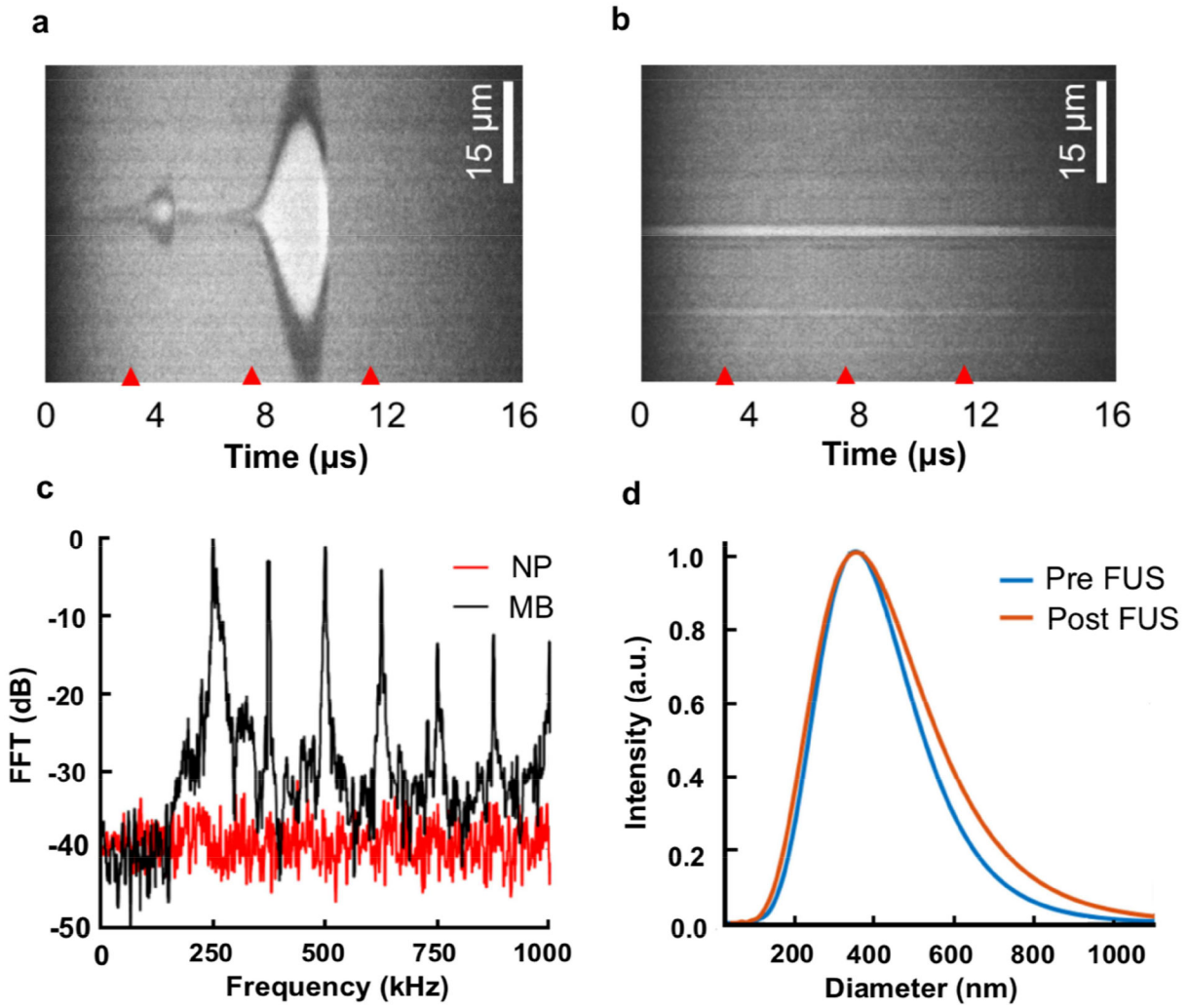

Fig. 7. PFP nanoemulsions undergo no observable oscillation or cavitation during sonication.

Ultra-high-speed camera streak images of **(a)** microbubbles (MBs), and **(b)** PFP nanoemulsions (NP) with sonication at a center frequency of 250 kHz. Red tick marks indicate the start of three cycles (4 μs) of the excitation waveform. **(c)** Magnitude of the received echo spectrum following excitation of the NPs (red line) and MBs (black line) as a function of frequency using 500 kPa peak negative pressure and a center frequency of 250 kHz with 150 ms pulses. **(d)** Size distribution of the NPs before (blue line) and after focused ultrasound (FUS) application (orange line).

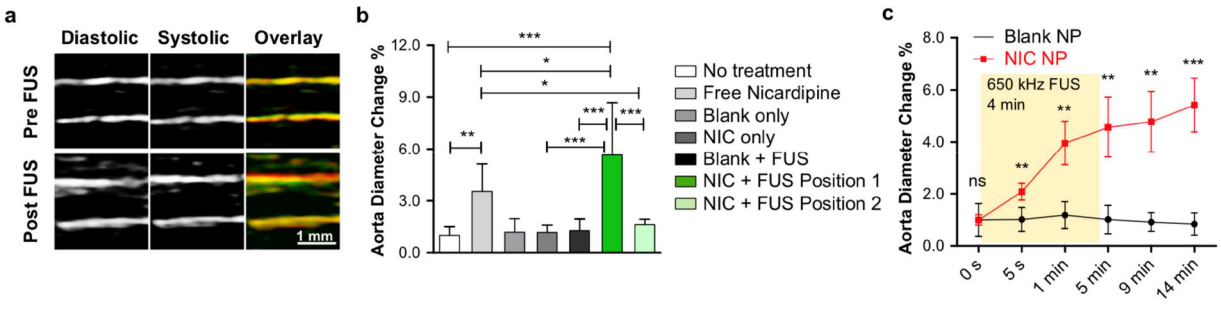

Fig. 8. Ultrasonic nicardipine uncaging increases local vessel compliance.

(a) Ultrasound images of the rat abdominal aorta during systole and diastole, before and after ultrasonic nicardipine uncaging (650 kHz, 240 repetitions of 50 ms pulses with 950 ms pauses, 1 Hz pulse repetition frequency, 1.5 MPa est. peak *in situ* pressure); green = diastolic, red = systolic, yellow = green/red overlap. Averaged rat abdominal aortic diameter at **(b)** 14 min after uncaging or **(c)** across time, normalized by the initial (0 s) values. FUS = focused ultrasound application, NIC = nicardipine-loaded nanoparticles. Free nicardipine and NIC administered to total drug dose of 134 μg/kg i.v. Mean +/− S.D. are presented for groups N=5–6 (**b, c**). ns: not significant, **: $p < 0.01$; ***: $p < 0.001$ by ANOVA and Tukey post-hoc tests (**b**, $F(6,30)=28.49$) or by two-tailed Student's t-tests between the nicardipine-loaded nanoparticles and the corresponding negative conditions (**c**).

Table 1.

Half-life of drug-loaded nanoemulsions fitted with two-phase decay modeling.

	Propofol		Nicardipine		Doxorubicin	
	$t_{1/2\alpha}$ (min)	$t_{1/2\beta}$ (min)	$t_{1/2\alpha}$ (min)	$t_{1/2\beta}$ (min)	$t_{1/2\alpha}$ (min)	$t_{1/2\beta}$ (min)
Whole blood	12.6	91.4	12.3	96.7	10.9	77.8
Plasma	26.4	117.2	22.1	142.5	19.8	129.6